

# IMPROVED ANALYTICAL CHIP THICKNESS MODEL

Lee Kumanchik and Tony L. Schmitz  
 Department of Mechanical and Aerospace Engineering  
 University of Florida, Gainesville, FL, USA

## INTRODUCTION

Discrete part production by macro- and micro-milling remains an important manufacturing capability. To improve process efficiency and part quality, research efforts continue with a focus on pre-process performance predictions. Important aspects of milling models include developing an accurate description of the system dynamics and cutting forces; see [1] for an overview. The cutting forces are generally taken to be a function of the time varying chip thickness. Therefore, a number of authors have studied chip thickness in milling and reported various models [2-7].

cutter teeth and radial runout. Expressions for entry and exit angles and limiting combinations of feed rate, spindle speed, and tool radius for chip formation are also provided. It is shown that the new model is more accurate than the well-known circular tooth path approximation and the analytical model presented in [6].

## NON-DIMENSIONAL TOOL PATH

The path of the  $i^{\text{th}}$  tooth in a milling cut can be described parametrically as:

$$\begin{aligned} x_i &= \rho\theta + r_i \sin(\theta + \phi_i), \\ y_i &= r_i \cos(\theta + \phi_i) \end{aligned} \quad (1)$$

where  $\rho = f/\omega = N_t f_t / 2\pi$  is the radius of the circle that defines the cycloidal motion of the tooth,  $f$  is the linear feed rate,  $\omega$  is the spindle speed,  $N_t$  is the number of teeth,  $f_t$  is the feed per tooth,  $r_i$  is the radius of the  $i^{\text{th}}$  tooth,  $\theta$  is the instantaneous cutter angle, and  $\phi_i$  is the angle between  $\theta$  and the  $i^{\text{th}}$  tooth. Figure 1 shows a schematic of the tool path and tool. Equation 1 can be written in non-dimensional form by dividing by the nominal tool radius,  $r$ , yielding:

$$\begin{aligned} x_i/r &= X_i = \varepsilon\theta + \alpha_i \sin(\theta + \phi_i) \\ y_i/r &= Y_i = \alpha_i \cos(\theta + \phi_i) \end{aligned} \quad (2)$$

where  $\varepsilon = \rho/r$  is the non-dimensional cutting parameter,  $\alpha_i = 1 + e_i$  is the non-dimensional tool radius of the  $i^{\text{th}}$  tooth which is nominally 1 but varies by  $e_i$ , and  $e_i$  is the runout of the  $i^{\text{th}}$  tooth normalized with the nominal radius  $r$ . For no runout, the non-dimensional tool path of any tooth is defined solely by  $\varepsilon$ . As  $\varepsilon$  increases, the tool path becomes more elongated and the chip thickness increases. A plot of the tool path for a two tooth cutter with various  $\varepsilon$  values is provided in Fig. 2.

## LIMIT OF CHIP FORMATION

The chip thickness in milling is defined as the distance between the current tooth's path and the previous tooth's path along the current tooth's edge. Figure 2c shows that, for the given

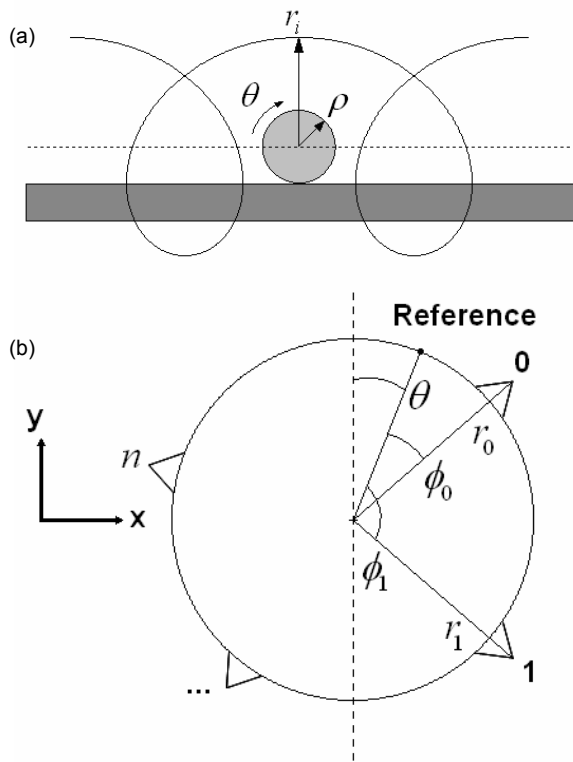


Figure 1: (a) Path for a tooth of radius  $r_i$  on circle of radius  $\rho$ . (b) Schematic of the milling tool. The reference,  $\theta$ , is common for all teeth; the difference in angular position for each tooth is the angle  $\phi$  which is measured from the reference.

In this work, we build on these previous studies to develop an analytical chip thickness model that incorporates the cycloidal trajectories of the

orientation, chip thickness is not defined. For the depicted orientation to be consistent with the definition for chip thickness,  $\varepsilon$  must be smaller so that the current tooth intersects the previous tooth's path as shown in Fig. 2b. The limit of chip formation is then the value  $\varepsilon_{\text{lim}}$  which allows all orientations of the current tooth in a cut to satisfy the chip thickness definition.

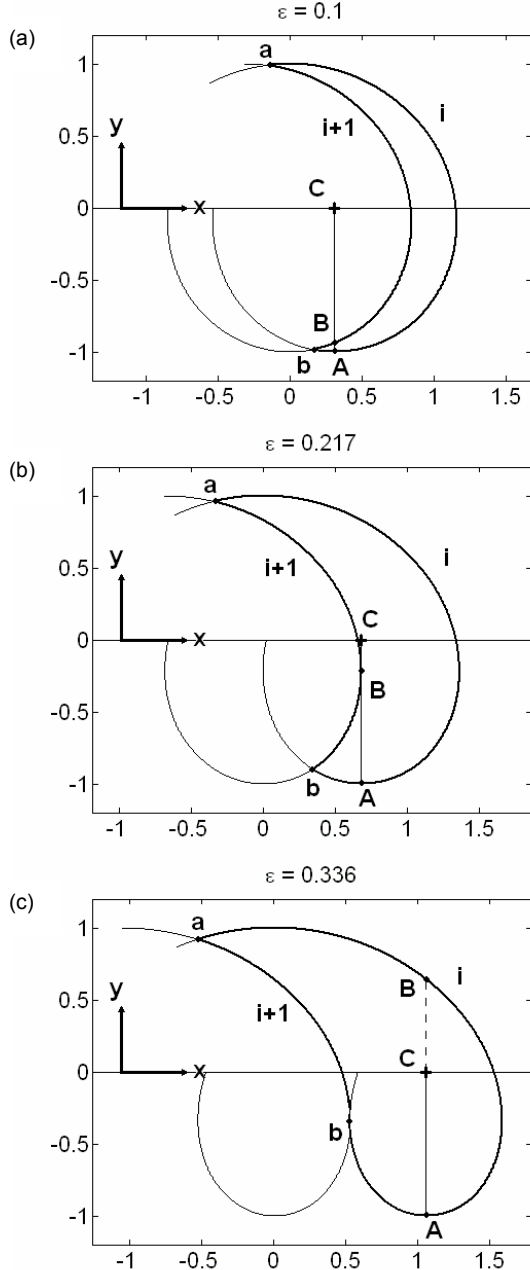


Figure 2: Non-dimensional tool path with increasing  $\varepsilon$ . Point **A** is the tooth tip, **B** is the intersection with the previous tooth's path, and **C** is the tool center. The outline of the chip being formed is identified.

As a first approximation of Fig. 2b, assume that the point of intersection, **B**, occurs on the line  $Y = 0$  so that at some point in time,  $t$ , the tooth,  $i+1$ , rotates onto the line  $Y = 0$  at the angle  $\theta_t + \phi_{i+1} = \pi/2$ . Later in time,  $t+1$ , the next tooth,  $i$ , rotates down to  $Y = -\alpha_i$  at  $\theta_{t+1} + \phi_i = \pi$ . For  $\varepsilon_{\text{lim}}$  these two locations share the same x-coordinate.

$$\begin{aligned}
 X_i(\theta_{t+1}) &= X_{i+1}(\theta_t) \\
 \Rightarrow \varepsilon\theta_{t+1} + \alpha_i \sin(\theta_{t+1} + \phi_i) &= \varepsilon\theta_t + \\
 &\quad \alpha_{i+1} \sin(\theta_t + \phi_{i+1}) \\
 \Rightarrow \varepsilon(\pi - \phi_i) + \alpha_i \sin(\pi) &= \varepsilon(\pi/2 - \phi_{i+1}) + \\
 &\quad \alpha_{i+1} \sin(\pi/2) \\
 \Rightarrow \varepsilon_{\text{lim}} &= \alpha_{i+1} / (\pi/2 + \phi_{i+1} - \phi_i) \quad (3)
 \end{aligned}$$

The limiting  $\varepsilon$  is a function of the angle difference between teeth on a tool and it increases for smaller teeth spacing. Evenly spaced teeth have the same angle difference for all teeth,  $\phi_{i+1} - \phi_i = 2\pi/N_t$ , but when considering unevenly spaced teeth the largest angle difference between any two consecutive teeth should be used. In addition,  $\varepsilon_{\text{lim}}$  is influenced by runout and so the value,  $\alpha_{i+1}$ , of the smallest tooth should be used. In reality the point of intersection, **B**, occurs when the tooth,  $i+1$ , has an x-direction velocity of zero:

$$\begin{aligned}
 X_{i+1}' &= \varepsilon + \alpha_{i+1} \cos(\theta_t + \phi_{i+1}) = 0 \\
 \Rightarrow \theta_t + \phi_{i+1} &= \arccos(-\varepsilon/\alpha_{i+1})
 \end{aligned}$$

The next tooth,  $i$ , still rotates to  $\theta_{t+1} + \phi_i = \pi$  and the x-coordinate of these two points are coincident:

$$\begin{aligned}
 X_i(\theta_{t+1}) &= X_{i+1}(\theta_t) \\
 \Rightarrow \varepsilon\theta_{t+1} + \alpha_i \sin(\theta_{t+1} + \phi_i) &= \\
 &\quad \varepsilon\theta_t + \alpha_{i+1} \sin(\theta_t + \phi_{i+1}) \\
 \Rightarrow \varepsilon(\pi - \phi_i) + \alpha_i \sin(\pi) &= \\
 &\quad \varepsilon \left[ \arccos(-\varepsilon/\alpha_{i+1}) - \phi_{i+1} \right] + \\
 &\quad \alpha_{i+1} \sin \left[ \arccos(-\varepsilon/\alpha_{i+1}) \right] \\
 \Rightarrow \varepsilon_{\text{lim}} &= \frac{\alpha_{i+1} \sin \left[ \arccos(-\varepsilon/\alpha_{i+1}) \right]}{\left[ \pi - \arccos(-\varepsilon/\alpha_{i+1}) + \phi_{i+1} - \phi_i \right]} \quad (4)
 \end{aligned}$$

Equation 4 must be solved numerically for a given angle difference. A plot of Eqs. 3 and 4 versus angle difference and the error between them is shown in Fig. 3. Most milling cuts have

values of  $\varepsilon$  that are far below the limiting value;  $\varepsilon_{\text{lim}}$  represents extremely aggressive cutting.

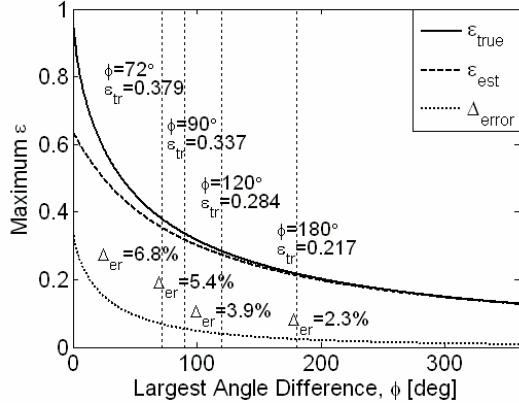


Figure 3: Maximum  $\varepsilon$  to still have normal chip formation given the angle difference between successive teeth. Smaller angle differences enable more aggressive cutting.

### ANALYTICAL CHIP THICKNESS

The chip thickness in milling,  $h$ , is the distance between the current and the previous tooth paths along the current tooth's edge (Fig. 2). The non-dimensional chip thickness is then:

$$\begin{aligned} \frac{h}{r} = H &= |AC| - |BC| = \alpha_i - |BC| \\ \Rightarrow H &= \alpha_i - \sqrt{\left( X_{i+1}(\theta_i) - X_C(\theta_{i+1}) \right)^2 + \left( Y_{i+1}(\theta_i) - Y_C(\theta_{i+1}) \right)^2} \\ H &= \alpha_i - \sqrt{\varepsilon^2 (\theta_i - \theta_{i+1})^2 + 2\varepsilon\alpha_{i+1}(\theta_i - \theta_{i+1})\sin(\theta_i + \phi_{i+1}) + \alpha_{i+1}^2} \end{aligned} \quad (5)$$

where  $|AC|$  and  $|BC|$  are the distance between points A and C, and B and C, respectively, in Fig. 2, and  $X_C$  and  $Y_C$  are the coordinates of the tool center ( $Y_C = 0$  always). As shown in [7] but rewritten in non-dimensional form, the relationship between  $\theta_{i+1}$  and  $\theta_i$  is:

$$\begin{aligned} (\theta_{i+1} - \theta_i)\varepsilon \cos(\theta_{i+1} + \phi_i) + \alpha_{i+1} \sin(\theta_{i+1} + \phi_i - \theta_i - \phi_{i+1}) &= 0 \end{aligned} \quad (6)$$

In order to make Eq. 5 a function of the current tooth's angle,  $\theta_{i+1}$ ,  $\theta_i$  must be solved numerically from Eq. 6 [7]. However, the sinusoidal term contains the angle difference between the current and previous teeth. Depending on  $\varepsilon$ , these two angles will be nearly

identical allowing the small angle approximation  $\sin \theta = \theta$  to be made in Eq. 6.

$$\begin{aligned} (\theta_{i+1} - \theta_i)\varepsilon \cos(\theta_{i+1} + \phi_i) + \alpha_{i+1}(\theta_{i+1} + \phi_i - \theta_i - \phi_{i+1}) &= 0 \\ \Rightarrow \theta_i &= \theta_{i+1} - \frac{(\phi_{i+1} - \phi_i)}{\varepsilon/\alpha_{i+1} \cos(\theta_{i+1} + \phi_i) + 1} \end{aligned} \quad (7)$$

Substituting Eq. 7 into Eq. 5 yields the non-dimensional chip thickness defined by  $\varepsilon$  and  $\alpha$  in terms of the current cutting tooth angle,  $\theta_{i+1}$ .

### ENTRY AND EXIT ANGLES

The entry and exit angles for a slotting cut can be determined by setting Eq. 5 equal to zero and using the substitution  $\theta_i - \theta_{i+1} = \phi_i - \phi_{i+1}$  based on the assumption that  $\theta_{i+1} + \phi_i \approx \theta_i + \phi_{i+1}$ ,  $H = 0$

$$\begin{aligned} \Rightarrow \alpha_i^2 &= \varepsilon^2 (\theta_i - \theta_{i+1})^2 + 2\varepsilon\alpha_{i+1}(\theta_i - \theta_{i+1})\sin(\theta_i + \phi_{i+1}) + \alpha_{i+1}^2 \\ \Rightarrow \alpha_i^2 &= \varepsilon^2 (\phi_i - \phi_{i+1})^2 + 2\varepsilon\alpha_{i+1}(\phi_i - \phi_{i+1})\sin(\theta_i + \phi_{i+1}) + \alpha_{i+1}^2 \\ \Rightarrow \theta_i + \phi_{i+1} &= \arcsin\left( \frac{\alpha_i^2 - \alpha_{i+1}^2 - \varepsilon^2 (\phi_i - \phi_{i+1})^2}{2\varepsilon\alpha_{i+1}(\phi_i - \phi_{i+1})} \right) \end{aligned} \quad (8)$$

The arcsine function in Eq. 8 is multivalued. To obtain the entry and exit angles that fall near  $\theta_i + \phi_{i+1} = 0$  and  $\theta_i + \phi_{i+1} = \pi$ , Eq. 8 can be written as two equations using the principal inverse sine function.

$$\begin{aligned} \theta_i + \phi_{i+1} &= \sin^{-1}\left( \frac{\alpha_i^2 - \alpha_{i+1}^2 - \varepsilon^2 (\phi_i - \phi_{i+1})^2}{2\varepsilon\alpha_{i+1}(\phi_i - \phi_{i+1})} \right) \end{aligned} \quad (9a)$$

$$\begin{aligned} \theta_i + \phi_{i+1} &= \pi - \sin^{-1}\left( \frac{\alpha_i^2 - \alpha_{i+1}^2 - \varepsilon^2 (\phi_i - \phi_{i+1})^2}{2\varepsilon\alpha_{i+1}(\phi_i - \phi_{i+1})} \right) \end{aligned} \quad (9b)$$

Equations 9a and 9b define the angle of the leading tooth,  $i+1$ , at chip entry and exit. If used with Eq. 2, they can describe the angle of the current tooth,  $i$ , by setting the y-equations for the different teeth equal to each other and solving for  $\theta_{i+1} + \phi_i$ :

$$Y_i(\theta_{i+1}) = Y_{i+1}(\theta_i)$$

$$\begin{aligned} \Rightarrow \alpha_i \cos(\theta_{i+1} + \phi_i) &= \alpha_{i+1} \cos(\theta_i + \phi_{i+1}) \\ \Rightarrow \theta_i + \phi_{i+1} &= \arccos\left(\alpha_i / \alpha_{i+1} \cos(\theta_i + \phi_{i+1})\right) \end{aligned} \quad (10)$$

The arccosine function in Eq. 10 is multivalued. To obtain the entry and exit angles that occur near  $\theta_{i+1} + \phi_i = 0$  and  $\theta_{i+1} + \phi_i = \pi$ , Eq. (10) is split into two equations using the principal inverse cosine function in combination with Eq. 9 (Eq. 11a for entry, 11b for exit).

$$\begin{aligned} \theta_i + \phi_{i+1} &= \\ &= -\cos^{-1}\left(\alpha_i / \alpha_{i+1} \cos\left((\theta_i + \phi_{i+1})_{9a}\right)\right) \end{aligned} \quad (11a)$$

$$\begin{aligned} \theta_i + \phi_{i+1} &= \\ &= 2\pi - \cos^{-1}\left(\alpha_i / \alpha_{i+1} \cos\left((\theta_i + \phi_{i+1})_{9b}\right)\right) \end{aligned} \quad (11b)$$

## RESULTS

In order to test the accuracy of the chip thickness equation developed here, comparison was made to other commonly used methods. The reference chip thickness was determined using the time domain simulation in [8]. The analytical methods tested were: the solution in this paper (linear), the circular tool path approximation (circular), and the solution developed in [6] (WIBT).

The first comparison was the difference in the average chip thickness over one revolution. The percent difference between each method as compared to the reference for a two tooth cutter is shown in Fig. 4a. The value  $\varepsilon$  in the plot is varied from near zero to the maximum,  $\varepsilon_{lim} = 0.217$ . All analytical solutions lose accuracy as  $\varepsilon$  increases; however, the solution provided here is most accurate. Figure 5b shows the positive error between the time domain and analytical solutions as a function of cutter angle.

## CONCLUSIONS

This paper presented an improved, non-dimensional chip thickness model that incorporates the cycloidal trajectories of the cutter teeth and radial runout.

## REFERENCES

1. Smith, S., and Tlusty, J., 1991, An Overview of Modeling and Simulation of the Milling Process, *Journal of Engineering for Industry*, **113**: 169-175.
2. Tlusty, J., and MacNeil, P., 1975, Dynamics of Cutting Forces in End Milling, *Annals of the CIRP*, **24**/1: 21-25.

3. Montgomery, D. and Altintas, Y., 1991, Mechanism of Cutting Force and Surface Generation in Dynamic Milling, *Journal of Engineering for Industry*, **113**: 160-168.
4. Spiewak, S., 1994, Analytical Modeling of Cutting Point Trajectories in Milling, *Journal of Engineering for Industry*, **116**: 440-448.
5. Spiewak, S., 1995, Improved Model of the Chip Thickness in Milling, *Annals of the CIRP*, **44**/1: 39-42.
6. Bao, W.Y. and Tansel, I.N., 2000, Modeling Micro-end-milling Operations, Part I: Analytical Cutting Force Model, Part II: Tool Run-out, *International Journal of Machine Tools and Manufacture*, **40**: 2155-2173, 2175-2192.
7. H.Z. Li and X.P. Li, 2005, A Numerical Study of the Effects of Cutter Runout on Milling Process Geometry Based on True Tooth Trajectory, *International Journal of Advanced Manufacturing Technology*, **25**: 435-443.
8. Schmitz, T., Couey, J., Marsh, E., and Tummond, M., 2004, The Role of Cutter Eccentricity on Surface Finish and Milling Forces, Proceedings of American Society of Mechanical Engineers International Mechanical Engineering Congress and Exposition, IMECE2004-60232, Anaheim, CA

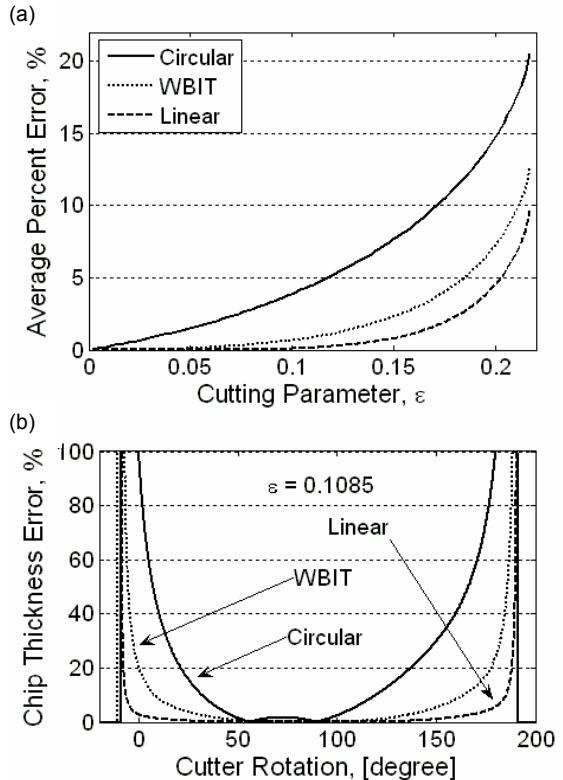


Figure 4: (a) Average error with increasing  $\varepsilon$ . (b) The positive error in chip thickness as a function of cutter angle for a two-flute cutter with  $\varepsilon = 0.1085$ .